Global optical model potential for elastic deuteron scattering from 12 to 90 MeV

W. W. Daehnick, J. D. Childs,* and Z. Vrcelj

Nuclear Physics Laboratory, University of Pittsburgh, Pittsburgh, Pennsylvania 15260

(Received 21 January 1980)

A set of about 4000 data points has been used in a global search for a general optical model parameter prescription. This potential for deuteron-nucleus scattering was confined to remain within the range given by folding model calculations. The data set spans the energy range from 11.8 to 90 MeV and includes many targets ranging in mass from ^{27}Al to ^{238}Th. The set includes 50 reaction cross sections, 13 angular distributions for vector polarization at and above 15 MeV, and 103 angular distributions for elastic scattering. A successful 11-parameter potential of the conventional form fits all data analyzed to about 18% rms. Two of these parameters, V_R and a_I, are functions of proton number and target mass, while five (V_R, a_o, W_S, W_D, V_{LS}) are smooth functions of bombarding energy. The remainder (r_o, r_I, r_c, r_{LS}, a_{LS}) are constants. A simple functional dependence for $a_I(A,Z)$ approximately reproduces the rapid changes in $\sigma(\theta)$ found experimentally for nuclei at or near neutron shell closure. A comparison with earlier work suggests that the optical model analyses furnish the rms radii for the real and imaginary potentials with little ambiguity. General agreement but with a somewhat larger scatter (10%) is also found for the real and the imaginary volume integrals deduced. However, little consistency is seen for the imaginary volume integral if the bombarding energy is below 15 MeV. The rms radii and volume integrals have a small but distinct energy dependence. It was found that the 11-parameter potential occasionally has difficulty delivering good simultaneous fits for cross sections and vector polarizations. This situation was improved by the addition of a small, three-parameter imaginary spin-orbit term, which in our global prescription required short range and very small diffuseness.

NUCLEAR REACTIONS $A(d,d)A$ for $27 \leqslant A \leqslant 238$, $11.8 \leqslant E \leqslant 90$ MeV. Optical model analysis. Deduced: global optical model parameter prescriptions, real and imaginary volume integrals, and rms radii.

I. INTRODUCTION

The understanding of deuteron-nucleus scattering has benefited greatly from the use of the folding ideas introduced by Watanabe[1] and from subsequent refinements of this approach.[2-7] More complicated effects like deuteron breakup, distortions of the internal wave functions, the Pauli principle, and nonlocality have been addressed in the more recent theoretical studies.[3-15] As a result, folding considerations have effectively removed the earlier discrete ambiguities for the real potential V_R described by Drisko and others[16,17] and have limited the ranges for the optical model parameters r_0, a_0, and r_I, which may be considered physically meaningful. This in turn greatly reduces the remaining continuous ambiguities in optical model fits to elastic scattering data. The nonlocality effects encountered, particularly in the treatment of deuteron breakup effects, indicate some energy dependence not only for the corresponding optical potential depths,[3-5] but also for such geometric parameters as radii and diffusenesses. However, the transition from the computed nonlocal folding potentials to equivalent energy dependent local ones is difficult. Some folding calculations have been compared directly to data sets for limited energy ranges,[5,6]

and fair agreement has been found at low energies where Coulomb effects are important or predominate. Other studies[14,8] make a direct comparison of folding calculations with data for a specific target (^{58}Ni) for deuteron energies up to 80 MeV. The agreement is quite acceptable; however, it is not yet of a quality which is expected routinely from typical optical model fits, nor, as we wish to show in this paper, of the quality obtainable from a global optical model prescription for a wide range of target mass and deuteron energy.

The difficulties underlying folding calculations have several sources. Austern[13] points out that the results of the so-called "adiabatic three-body" approach (e.g., Ref. 3) in some cases differ appreciably from a more rigorous three-body treatment. Another uncertainty arises from the use of phenomenological nucleon-nucleus potentials in the folding integrals. Although the theoretical construction of nucleon-nucleus potentials is considerably further advanced than that for complex projectiles (e.g., Refs. 18 and 19), it has not yet reached the state where they can fully supplant empirical potentials. For instance, they still inadequately predict the energy dependence for the real volume integral for scattering of protons above 60 MeV.[20] Available phenomenological proton-nucleus po-

tentials[20-22] are very successful in their respective energy ranges. Nevertheless, they differ in important parameters such as real radius (1.15 to 1.25 fm), imaginary radius (1.25 to 1.5 fm), spin-orbit geometry, etc. This variation will necessarily be reflected in the folded deuteron potentials.

There remain many calculations, for instance those in the distorted wave Born approximation (DWBA), where one would be inclined to turn to empirical potentials for realistic deuteron phase shifts. Often consistency in the DWBA analysis requires also that even those phase shifts poorly determined in elastic scattering (but important in other reactions) be obtained in a systematic and optimal way.[23] These requirements often have been met by a good global optical model prescription. To the extent that such potential prescriptions fit data well they also correlate and systematize large amounts of empirical knowledge. Some historical average deuteron parameter sets (e.g., those of Refs. 17, 24, 25, 6, and 26) have proven very useful for these reasons. Their major shortcoming, as we found, is that an extrapolation to energies outside their data bases is not very successful. Hence the inclusion of higher energy data in a broad based analysis is called for. Our goal has been a systematic optical model description of elastic scattering for deuteron energies above 11.8 MeV where adequate data exist, i.e., up to 90 MeV, and over as wide a mass range as experience made seem advisable. We found that in general it was not difficult to constrain our parameters to values reasonable in the light of the available folding calculations.

II. OPTICAL MODEL CALCULATIONS FOR ELASTIC DEUTERON SCATTERING

A. Prior work

A large number of deuteron scattering experiments has been reported in the literature[6,24-44] in the energy range of interest. In most of the studies listed a limited number of isotopes was investigated at one particular energy in the region from 11.8 to 90 MeV. Concurrent or subsequent optical model[45] analyses were successful in fitting subsets of the known data with reasonable parameters.[5,6,16,17,24-26,46-48] A complete compilation of (d,d) optical model work before 1976 is given in Ref. 49. Here a brief summary of the earlier results may suffice. In optical model studies it has been customary to use a complex central potential of the Woods-Saxon shape and its derivatives, a spin-orbit term of

the Thomas form, and a Coulomb term. Hence the optical potential has been written as

$$V(r) = -V_R f(r, r_0, a_0) + i4a_I W_D \frac{d}{dr} f(r, r_I, a_I)$$

$$- iW_S f(r, r_I, a_I)$$

$$+ V_{LS} \left(\frac{\hbar}{m_\pi c}\right)^2 (\vec{L} \cdot \vec{S}) \frac{1}{r} \frac{d}{dr} f(r, r_{LS}, a_{LS}) + V_{\text{Coul}},$$

where the Woods-Saxon well f is given by

$$f(r, r_i, a_i) = \left[1 + \exp\left(\frac{r - r_i A^{1/3}}{a_i}\right)\right]^{-1};$$

A is the target mass number. The square of the pion Compton wavelength $(\hbar/m_\pi c)^2 = 2.00$ fm^2 is a conventional normalization factor. The Coulomb term is taken as the potential for a uniformly charged sphere of radius $R_c = r_c A^{1/3}$.

The search codes can vary any specified combination of potential parameters such that χ^2, a quality of fit quantity, is optimized. This quantity is defined as

$$\chi^2 = \frac{1}{N} \sum_{i=1}^{N} \left(\frac{\sigma_i^{\text{th}} - \sigma_i^{\text{exp}}}{\Delta \sigma_i^{\text{exp}}}\right)^2.$$

The quantities V_i, W_i, r_i, and a_i define four potential and six geometric parameters that can be varied in a fitting calculation. The Coulomb radius $R_c = r_c A^{1/3}$ is an eleventh parameter which is not very sensitive and rarely changed. More recently a tensor potential has been added to $V(r)$, and V_{LS} has been permitted to be complex (e.g., Refs. 50, 5, and 43). In most searches fewer than ten parameters are varied, and this has proved adequate to give an excellent reproduction of deuteron scattering below 90 MeV. However, a glance at the compilation of Ref. 49 shows a great diversity of "best-fit" parameters. Perey and Perey[17] in their pioneering 1963 study were able to find several equivalent families of similar best-fit parameters which gave good fits to data from 11.8 to 27 MeV. They also deduced an averaged parameter set (without spin-orbit term) which fit their entire data set to 25–30% on the average (rms deviation). In 1968 this low energy study was supplemented by Hinterberger et al.[24] by the analysis of their 52 MeV data. Taking into account the results of the 34 MeV study by Newman, Becker, and Preedom at Oak Ridge,[25] Hinterberger was able to propose an averaged parameter set, including a spin-orbit term which provided fits of similar quality to Perey's for the wider energy range of 12 to 52 MeV. Checking with our corresponding data set we find about 28% for the average root mean square deviation. Both studies achieved the wide

range of usefulness of their parameter sets by determining and parametrizing the A and E dependence in their best-fit parameters and making this a part of their global parameter prescription. Lohr and Haeberli[6] proposed an average parameter set for their 9–13-MeV scattering and polarization data. Their prescription gave no energy dependence and proposed a different A dependence for the imaginary term. It produced very good fits to the low energy polarization measurements. We find, however, that their prescription is not very successful outside the energy range for which it was constructed. A similar restriction applies to the averaged parameter set of Perrin *et al.* for their 29-MeV scattering and polarization data,[26] and to a number of earlier studies. In 1973 we began compiling a comprehensive data set which included a wide range of bombarding energies and was meant to be analyzed with the global search code GENOA, written by Perey.[51] As a first step an attempt was made to resolve experimental discrepancies[17] for the early 15-MeV data by careful measurement of 23 angular distributions for medium weight and heavy targets at 17 MeV.[38] In the subsequent global analysis of the 17-MeV data it was found that very acceptable fits could be obtained with a single set of parameters.[52] An extension of this parameter set to higher and lower energies (12–52 MeV) also proved successful after (a linear) energy dependence in the V and W parameters was introduced.[52,53] When (d, d) scattering data in the 80–90-MeV energy range[39–41] were compared with the early prescriptions, it was found that the potentials of Refs. 52 and 53 reproduced the higher energy data in a qualitative way. Typical rms deviations were ±40%. This was better than for other available global prescriptions, but much worse than the ±25% fits obtained for the data at 52 MeV and below.

B. Data sets for a global search

Historically, optical model best-fit parameters have shown variations with beam energy E and target mass A. It has also been noted from the beginning that good systematic fits at low energy (<30 MeV) were very difficult to find for targets with $A < 40$. Even at the higher energies of 60–90 MeV it has been found[40,41] that scattering from light targets such as ^{12}C and ^{24}Mg must be analyzed with a coupled channels mechanism that takes explicit account of the strong inelastic scattering channel. The search code GENOA (Ref. 51) will handle 1000 data points at a time, and it was decided to incorporate a carefully selected subset of all available data into the data

sets for our global searches. Eliminated from consideration were all data for bombarding energies below 11.8 MeV and almost all data for targets lighter than aluminum ($A = 27$). An exception was made for cross sections for energies at and above 80 MeV where elastic scattering data are scarce and where compound-elastic effects are unimportant. The existence of important two-step effects[40,41] was taken into consideration by weighting the ^{12}C and ^{24}Mg entries less than other data (i.e., at 50%). A similar, reduced weighting was used for a few targets of high deformation (^{232}Th and ^{238}U) if strong low-lying excited states were not resolved experimentally. It seemed advisable to not completely ignore such data because they could expand the mass range investigated down to $A = 12$ and up to $A = 238$. Generally, in our selection, the more systematic and more recent studies were preferred, especially if accurate numerical data had been published or could be obtained.

Included from the beginning were 21 angular distributions at 11.8 MeV from Heidelberg,[27] 23 angular distributions at 17 MeV from Pittsburgh,[38] 16 angular distributions at 34 MeV from Oak Ridge,[25] and 18 angular distributions at 52 MeV from Karlsruhe.[24] At later dates the global search sets were expanded by the inclusion of six vector polarization angular distributions at 15 MeV from Los Alamos,[54] five at 30 MeV from Grenoble,[55] and two at 79 MeV from Indiana.[42]

Most 80–90 MeV data[39–41,44] were not available in numerical form and had to be read off the graphs in the publications cited. Although done with care, this method introduced additional errors estimated at up to 10%. It was noticed that the near duplicate data available for ^{12}C and ^{27}Al had normalizations (see Refs. 39, 40, and 44) that disagreed by factors so far outside statistical or ordinary experimental uncertainties that one or the other of these early measurements had to be in error. In the absence of more objective criteria we looked for systematic (dis)-agreement at angles below 30° with global optical model parameters for other targets at similar energies. By this criterion the absolute ^{12}C normalization of Ref. 40 appeared in error. It was increased by a factor 1.58, whereas that of Ref. 39 was left unchanged. For ^{27}Al the normalization of the more recent study of Ref. 44 seems to be correct. It was left unchanged, but the ^{27}Al cross sections of Ref. 39 were renormalized by a factor 0.55. A smaller, but less trivial, systematic error seems to exist for the ^{58}Ni curve of the same study. This cross section was remeasured as part of a recent polarization study at the same energy.[42] After finding

the expected disagreements with the earlier study, we excluded the older ^{58}Ni curve from our searches and used the new one. Hence the current 80–90-MeV set contains five angular distributions at 80 MeV from Orsay,[39] six angular distributions at 85–90 MeV from Julich,[40, 41, 44] and four angular distributions at 79–79.5 MeV from Indiana.[42]

The distribution in A and E of the data in our search sets is illustrated in Fig. 1. Thirteen of the 106 angular distributions are for vector polarization $P(\theta)$, $[P = (2/\sqrt{3})iT_{11}]$, the remainder for elastic cross sections. The total number of data points used is slightly below 4000. This number is somewhat lower than the total number of points available for the 106 angular distributions and results from the dropping of alternate points in overdetermined cross sections with little structure, mostly for In to Th at 11.8 MeV, where fits are easy to obtain and provide little information. The statistical errors for most data points are 1–2%, but always below 5%. Hence the errors significant for the global analysis are generally of a systematic nature (errors in absolute normalization and the uncertainty in the scattering angle θ for the higher energies). It appears that most data sets have systematic errors of about 10%. For the purpose of the global searches, we assigned equal (5 or 10%) errors to all data points at a given energy and treated them as if they were random. This assumption would be poor for the analysis of one individual angular distribution. However, for the entire set of 106 angular distributions it seems reasonable to assume that the cross section normalization errors and typical angle

Map of Targets and Energies Searched

FIG. 1. Graphic display of the data set used in this study. Targets are indicated by their mass A. The E axis denotes the deuteron bombarding energy. Data with energies below 11.8 MeV were not included. The exclusion of data for targets with $A < 27$ at the lower energies is explained in the text. Of 106 angular distributions included, 13 are for vector polarization.

calibration errors have a random variation from one angular distribution to the next. Because of the scarcity of data near 80 MeV the high energy data (except ^{12}C and ^{24}Mg) were weighted twice as heavily as the low energy points. This intentional bias might lead to better fits in the 80–90-MeV region and slightly poorer ones at 52 MeV than with uniform weighting. Of course, as with any limited data set, we may still have unintentional biases in our search of which we have remained unaware.

C. Search procedure

The typical search for our 4000 data points required five parallel GENOA runs. We tended to use five free global parameters at a time with five to six successive variations for good convergence. The CPU time at the Pittsburgh DEC1090 computers for such a search of the complete data set totals 36 min. This relatively modest cost permitted us to make many searches over a span of several years. Historically the following search procedure was followed. Starting with optical potentials closely analogous to those obtained from an adiabatic folding approach[5,2] individual best-fit parameters for all 17-MeV angular distributions were found. Generally, the variation of nine parameters was needed to obtain fits within the experimental accuracy over the full angular range (5° to 165°). Best-fit r_0 values for the 17-MeV data fell between 0.91 and 1.17. The ranges of the other best-fit parameters[38] were $92 < V_0 < 114$ MeV, $0.71 < a_0 < 0.96$, $8.7 < W_D < 16.7$, $1.27 < r_I < 1.46$, $0.64 < a_I < 0.86$, $5.63 < V_{so} < 13.5$, $0.7 < r_{so} < 1.4$, $0.3 < a_{so} < 1.85$. A similarly large variance is found for unconstrained best-fit parameters at 85 MeV, although here r_0 tends to stay above 1.15, a_0 above 0.81, and r_I below 1.30. All parameters were subject to continuous ambiguities which, however, had limited and differing ranges. We next restricted the geometric parameters to ranges consistent with the adiabatic folding models. In particular, real radius parameters below 1.1 fm and above 1.20 fm were not admitted in the searches. This restriction saved a lot of computer time and does not seem to have excluded above average fits. Similarly, only such V_R values were tried which would keep the real volume integrals within the range (300–450 MeV fm^3) predicted by folding calculations.

D. Global fits for 11.8–52-MeV differential cross section data

Because our version of GENOA cannot handle more than 30 angular distributions (or 1000 points) simultaneously for a given search, the data were first organized and searched on ac-
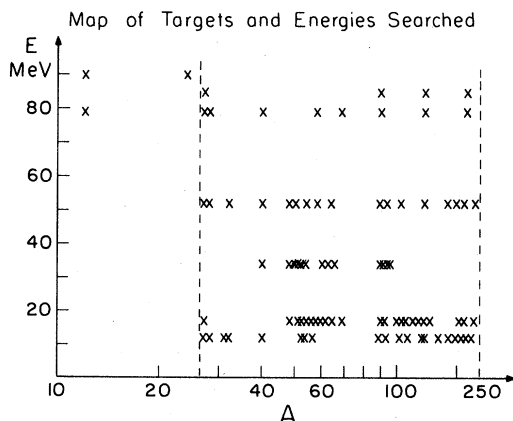
cording to their deuteron beam energies. Each search started with a similar parameter prescription. The well converged parameter values were then plotted against energy to construct a general global formulation. Initially it was found that there was a very clear energy and A dependence in the depth of the real potential, as well as in the diffuseness of the imaginary potential. In analogy to earlier work,[17,24,6] we introduced the parametrization $V_R = V_0 - a_2 E + a_3 Z/A^{1/3}$ and $a_I = a_8 + a_9 A^x$. It was found, particularly from the analysis of the 17–52-MeV data, that with the constraint of global parameters, $x = \frac{1}{3}$ provided the best approximation.

From the beginning of the analysis it was recognized that any global fits to deuteron elastic data on a number of different targets would be hampered by target-dependent structure effects. In particular, for our 17-MeV cross section data we had observed that for a fixed real geometry the imaginary geometry parameters were noticeably affected by the fullness of the shells. With hopes of isolating the one imaginary potential parameter that could be correlated most clearly with shell effects, each of the three parameters (W_D, r_I, and a_I) was allowed to go free as the other two parameters were kept global. The only parameter of the three showing any striking and simple target structure dependence was the imaginary diffuseness a_I.

A number of attempts were made to correlate imaginary geometry behavior with known structure effects. At various times, we considered in turn the deformation parameter β, the $BE(2)$ values,[33] the ground state mass excesses, and the excitation energies of the first 2^+ state. Some systematic correlation with the imaginary potential was observed, but no single functional dependence could be used for a wide mass and energy range.

The observed behavior of a_I near closed shells led us to the introduction of a shell structure (magic number) term in the imaginary diffuseness a_I,

$$a_I = a_{I_0} - k \sum_i \exp\{-[(N - M_i)/\delta]^2\},$$

where k is the strength of the shell effect (~ 0.05) at closed *neutron* shells, δ is the "width" of the shell term around the closed shell in units of neutron number, and the index i designates the magic numbers (so that $M_i = 8$, 20, 28, 50, 82, and 126). This self-contained formula proved adequate in accounting for the more pronounced structure effects in our subsequent fits.

The neutron shell closure behavior was a very striking property of the 17-MeV data as

well as the 11.8-MeV data and the 34-MeV data. The 52-MeV data displayed less of this kind of magic neutron shell systematics. It is plausible that such shell effects would be important at lower energies but become less prominent as the bombarding energy is raised. Attempts were made to incorporate a similar structure term which would reduce a_I at the closed proton shells. However, when the data base was expanded from 17 MeV to include the other energies, the global searches rejected such a term.

Many of our subsequent global searches were performed on three data sets organized by neutron number, i.e., one set contained only targets at all energies with magic neutron numbers, a second set included targets whose neutron numbers are "close" to a magic number ($1 \leq |N - N_{\text{magic}}| \leq 5$), and a third set included targets whose neutron numbers are "far" from a magic number ($|N - N_{\text{magic}}| > 5$).

Initially the fitting was performed with only a surface-peaked imaginary potential W_D. Since one expects volume contributions to the absorption to become more significant with increasing energy,[18] it was logical to include a volume imaginary potential which would share the same geometry as the surface term. It was further hoped that by letting these imaginary depths become energy dependent, as the folding models predict, the energy term in the imaginary diffuseness could be eliminated. In general, one would prefer that geometric parameters like a_I would be constant with energy.

Searches were made at each energy with an energy-independent a_I and fixed r_I. The resulting imaginary depths showed the expected behavior: the surface term dominated at low energies while the volume term became more important at 52 MeV and was most important at 85 MeV. Although the inclusion of energy-dependent volume and surface imaginary terms was essential for good fits over a reasonable energy range, the precise relative strengths and energy dependences were *not* well established by the data. It was observed that the change with E from surface to volume absorption could be made more or less gradual without any considerable change in the fits. The inclusion of the 80–90-MeV data helped reduce this ambiguity considerably.

Three potentials were obtained from fits to the 11.8–52-MeV differential cross section data[52] which we label A, B, and C. They are distinguished by their (fixed) real radius values of 1.1, 1.15, and 1.2 fm, respectively. They are listed in Table I, along with the other early prescriptions for global potentials. The quality of their

TABLE I. A comparison of global optical parameter prescriptions used previously. The potential names indicate the year the prescription was first available, names of authors, and energy range of the data base which was fit, or to which it was adaptable. The listing is for comparison purposes only. For most purposes these potential forms are superseded by those listed in Table III. See text and Table II. A = mass number, Z = proton number, N = neutron number, $\alpha = -(E/91.7)^2$, $\mu_i = [(M_i - N)/2]^2$, where M_i = magic number (8, 20, 28, 50, 82, 126). E = deuteron laboratory energy in MeV. CD = Ref. 52, VRC = this work.

Name	V_R (MeV)	r_0 (fm)	a_0 (fm)	W_S (MeV)	W_D (MeV)	Data fitted
(63) Perey 11.8–27 MeV	$81-0.22E$ $+2.0ZA^{-1/3}$	1.15	0.81	0	$14.4+0.24E$	$\sigma(\theta),\ \sigma_R$
(68) Hinterberger 34–52 MeV	$79-0.35E$ $+1.5ZA^{-1/3}$	1.25	0.81 $-0.024A^{1/3}$	0	13.0	$\sigma(\theta)$
(74) Lohr and Haeberli 9–13 MeV	$91.13+2.2ZA^{-1/3}$	1.05	0.86	0	$218A^{-2/3}$	$\sigma(\theta),\ P(\theta)$
(76) Perrin with $V(E)$ 9–34 MeV	$(88.04-0.26E)$ $+1.77A^{-1/3}$	1.13	0.80	0	12.0	$\sigma(\theta),\ P(\theta)$
(76) CD, 11.8–52 MeV, A	$93.4-0.235E$ $+1.2ZA^{-1/3}$	1.10	0.825	$0.08(E-17)$	$14.58-0.07E$	$\sigma(\theta)$
(76) CD, 11.8–52 MeV, B	$89.05-0.23E$ $+1.0ZA^{-1/3}$	1.15	0.79	$0.063(E-17)$	$14.9-0.066E$	$\sigma(\theta)$
(76) CD, 11.8–52 MeV, C	$84.0-0.196E$ $+0.79ZA^{-1/3}$	1.20	0.751	$0.046(E-17)$	$15.3-0.062E$	$\sigma(\theta)$
(76) CD, 11.8–52 MeV, D	$89.05-0.23E$ $+1.0ZA^{-1/3}$	1.15	0.78	$0.063(E-17)$	$14.9-0.066E$	$P(\theta),\ \sigma(\theta)$
(76) CD, 11.8–52 MeV, E	$89.05-0.23E$ $+1.0ZA^{-1/3}$	1.15	0.79	$0.063(E-17)$	$14.9-0.066E$	$\sigma(\theta),\ P(\theta),\ \sigma_R$
(79) VRC, 11.8–90 MeV, C' (relativistic kinematics)	$86-0.285E$ $+0.88ZA^{-1/3}$	1.20	0.755	$15.9(1-e^{\alpha})$	$15.0e^{\alpha}$	$\sigma(\theta)$

Name	r_I (fm)	a_I (fm)	r_C (fm)	V_{LS} (MeV)	r_{LS} (fm)	a_{LS} (fm)
(63) Perey 11.8–27 MeV	1.34	0.68	1.15	0		
(68) Hinterberger 34–52 MeV	1.25	$0.51+0.076A^{1/3}$	1.30	6.0	1.25	0.81 $-0.024A^{1/3}$
(74) Lohr and Haeberli 9–13 MeV	1.43	$0.50+0.013A^{2/3}$	1.30	7.0	0.75	0.50
(76) Perrin with $V(E)$ 9–34 MeV	$1.15+0.75A^{-1/3}$	$0.585+0.05A^{1/3}$	1.30	5.2	0.85	0.475
(76) CD, 11.8–52 MeV, A	1.35	$0.414+0.088A^{1/3}$ $-0.031\sum_i e^{-\mu_i}$	1.30	7.3	0.98	1.0
(76) CD, 11.8–52 MeV, B	1.33	$0.443+0.082A^{1/3}$ $-0.034\sum_i e^{-\mu_i}$	1.30	7.1	0.98	1.0
(76) CD, 11.8–52 MeV, C	1.31	$0.478+0.075A^{1/3}$ $-0.044\sum_i e^{-\mu_i}$	1.30	6.8	0.98	1.0
(76) CD, 11.8–52 MeV, D	1.33	$0.528+0.064A^{1/3}$ $-0.025\sum_i e^{-\mu_i}$	1.30	5.7	1.10	0.55
(76) CD, 11.8–52 MeV, E	1.33	$0.448+0.082A^{1/3}$ $-0.043\sum_i e^{-\mu_i}$	1.20	5.5	1.10	0.55
(79) VRC, 11.8–90 MeV, C' (relativistic kinematics)	1.31	$0.495+0.064A^{1/3}$ $-0.052\sum_i e^{-\mu_i}$	1.30	$\dfrac{9.73}{(1+0.0095E)^2}$	1.10	0.55

fits to the 11.8–52-MeV data can be assessed by comparing Table II with Figs. 2–5.

The spin-orbit geometry for these potentials was held fixed to that predicted by a folding calculation.[5] However, with each potential, V_{LS} was allowed to vary. Differential cross section data do not, by themselves, accurately determine the spin-orbit potential. Nevertheless, such a potential was needed to help fit the high angle cross sections for many targets.

E. Fits of polarization data

In order to cross check and to better determine the parameters of the spin-orbit potential it was decided to use the available vector polarization data at and above 15 MeV.

First, we fitted the polarization data by themselves starting with the ($r_0 = 1.15$) potential B which used the folding prediction for the spin-orbit geometry, $r_{LS} = 0.98$ fm and $a_{LS} = 1.0$ fm. Letting the spin-orbit depth go free, the χ^2 improved by a factor of 2 as V_{LS} settled on very low values of 2.1 to 2.4 MeV. When all three spin-orbit parameters were allowed to vary, even further improvements in χ^2 were obtained (about 30%) as the spin-orbit radius r_{LS} increased to 1.1 fm, the diffusivity a_{LS} halved in value to 0.55 fm, and the depth V_{LS} settled into

the range of around 5.5 MeV. Next we included both the differential cross section sets *and* the 15- and 30-MeV polarization sets in the search. The resulting potential, known as potential D, is found in Table I. Potential D represents about a 15% increase in the total χ^2 for differential cross section data with an improvement by about a factor of 2 in the total χ^2 for polarization data, compared to the fits with potential B.

Up to this point, our polarization searches were done with a spin-$\frac{1}{2}$ formalism. [Comparisons of selected 12- and 17-MeV polarization predictions between spin-$\frac{1}{2}$ and spin-1 calculations had indicated remarkably little difference, except for the rescaling (by $\frac{4}{3}$) of the spin-orbit depth V_{LS} itself.] The 30-MeV (and 80-MeV) polarization predictions, however, displayed more significant differences between the two formalisms, primarily concerning the amplitude of oscillations, particularly for the heavier nuclei.

Hence, polarization searches for the higher energies were always checked (or redone) with a spin-1 formalism. Because the search code GENOA permits only spin-$\frac{1}{2}$ calculations, it was necessary to perform the searches either by doing a series of single-shot calculations using a spin-1 code (DWUCK) or by using the search

TABLE II. The success of several popular global prescriptions in fitting the current set of data is quantified in terms of χ^2 values found. These χ^2 values are tabulated below, together with χ^2 values of potentials presented in this paper. For $\sigma(\theta)$, $\chi^2 = 1$ means an rms data-theory difference of 10%; $\chi^2 = 4$ implies an rms difference of 20% between data and predictions. The names of the parameter sets indicate year of availability, author, energy range of expected validity, and letter $A–L$ label. As can be seen from Tables I and III, the potentials become more complicated towards the bottom of the list. The χ_{av}^2 values for fits to the vector polarization are approximate and are based on $\Delta P_i(\theta) = \pm 0.05$. Generally, asymmetry data are more accurate. For most potentials the 15-MeV polarizations are fit poorly. [The situation is reversed for the (74) Lohr potential. Here the fits are very good with $\chi^2 \approx 3.4$ for the 15-MeV data, but close to 48 for the 30-MeV data. We were not able to generalize the Lohr potential with a function $V_R(E)$, as proved possible for the Perrin potential.] $(\chi^2)_{av} = (1/N) \sum_{i=1}^{N} [(\sigma_i^{th} - \sigma_i^{exp})/\Delta\sigma_i^{exp}]^2$; $\Delta\sigma_i = 0.1\sigma_i$; $\Delta P_i = 0.05$.

| Deuteron energy Parameter sets	11.8 MeV	17 MeV	34 MeV	52 MeV	85 MeV	Pol. 15, 30 MeV	Pol. 80 MeV
Historical sets							
(63) Perey and Perey 11.8–27 MeV	5.3	10.1	(47.5)	(95)	(494)	no $L \cdot S$	no $L \cdot S$
(68) Hinterberger 34–52 MeV	4.65	6.6	10.8	8.9	(82.6)	16	(75)
(74) Lohr and Haeberli 9–13 MeV	2.04	12.1	(148)	(17 667)		20	(276)
(76) Perrin with $V(E)$ 9–52 MeV	4.3	4.9	14.9	(69.8)	(99.5)	7.5	(190)
(76) CD, 11.8–52 MeV, A	2.89	2.84	6.09	5.32	11.7	10	(106)
(76) CD, 11.8–52 MeV, B	3.06	2.75	6.07	5.31	11.6	9.0	(92)
(76) CD, 11.8–52 MeV, C	3.09	2.96	6.87	5.49	15.9	9.3	(87)
(76) CD, 11.8–52 MeV, D	3.16	3.51	5.99	6.82	25.8	5.2	(80)
(76) CD, 11.8–52 MeV, E	3.35	3.36	6.06	5.87	19.9	5.9	(53)
(79) VRC, rel, 11.8–90 MeV C'	3.49	3.08	7.70	6.84	4.28	9.2	(34)
Current-this work							
(79) DCV, rel, 11.8–90 MeV, F	2.46	2.57	5.54	4.00	2.9	6.8	3.9
(79) DCV, nonrel, 11.8–90 MeV, L	2.51	2.44	5.37	3.99	3.1	7.4	3.0
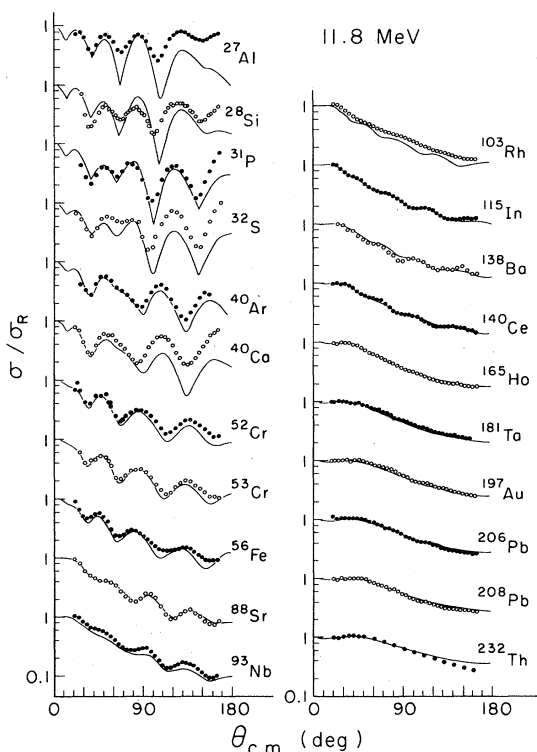
FIG. 2. Comparison of the 11.8-MeV data $[\sigma(\theta)_{exp}/\sigma_{Rutherford}]$ of Ref. 27 with the predictions of the global potential L (Table III). Nearly identical agreement was obtained for potential F. Slightly better fits would be provided by the low energy potential of Lohr (Ref. 6) and slightly inferior fits are obtained from potentials A, B, C, D, E, and VRC. (See Table II for a quantitative comparison.) If allowance is made for the $\sigma/\sigma_{Rutherford}$ presentation it is seen that the difference between data and theory for targets up to ^{52}Cr is nearly independent of angle as might be expected from S-wave compound elastic scattering contributions. For ^{103}Rh and ^{232}Th inelastic cross sections to one or more low-lying excited states may be included in the data.

FIG. 3. Comparison of the 17-MeV elastic scattering data of Ref. 38 with the predictions of the global potential L. Fits with potentials F and F' are nearly identical. See Table II for a quantitative comparison of fits to these data by other global prescriptions.

code CUPID.[56] This modified global potential was then refit to the differential cross section data, which resulted in a slight readjustment of the structure term in the imaginary diffuseness a_I. In addition, setting $r_C = 1.2$ fm resulted in a slight change in the real depth V_R. This potential which fits differential cross sections and polarization data from 11.8 to 52 MeV was labeled potential E (see Table I). The quality of the polarization fits is similar to potential D, but it does a better job for the 52-MeV cross section data (see Table II).

F. Inclusion of 80–90 MeV data

An adequate set of 80–90-MeV cross sections was obtained fairly late in this study. The first 80-MeV polarization data did not become avail-
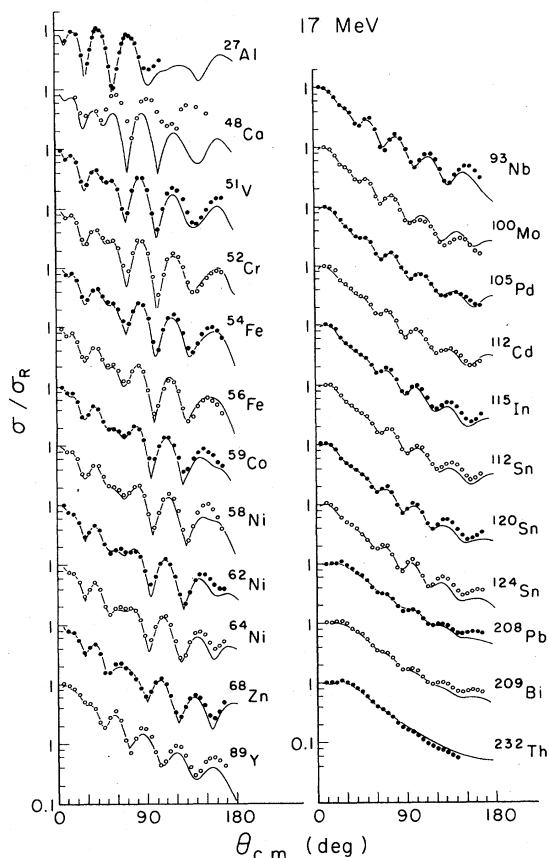
able until summer, 1979.[42] It then became apparent that none of the earlier global prescriptions produced good predictions at 80 MeV. The overview of Table II shows that our potentials A, B, and C gave agreement to within 35–45% (rms deviation), which falls far short of the quality of the fits at lower energy. A search on the "85-MeV" set starting with potentials B or C indicated the need for changes in a_0, r_I, and in the spin-orbit potential V_{LS}. As a minimum, V_{LS} had to be made energy dependent. It turned out that a reasonable extension of potential C was possible if relativistic kinematics were used in the computations. This potential has been named C' and is listed in Table I. Table II shows that potential C' extends the range of usefulness to 85 MeV at a modest cost in fit accuracy at the lower energies, but still fails to fit the 80-MeV polarization data.

Ultimately it was decided to take a second look at the energy dependence of critical parameters
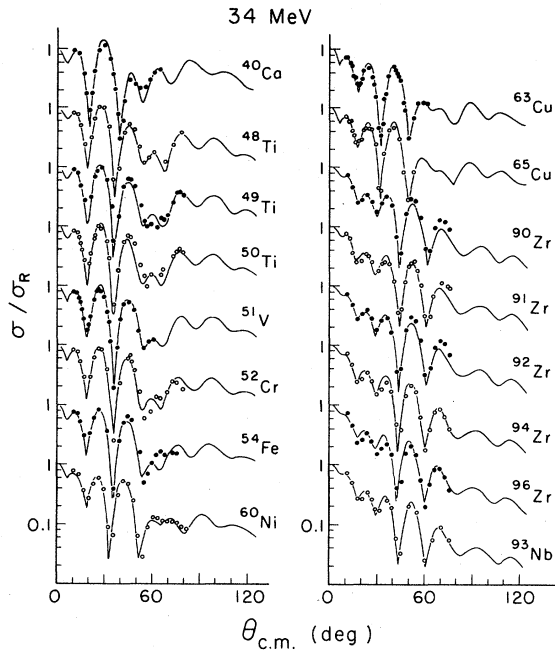
FIG. 4. Comparison of the 34-MeV data of Ref. 25 with the predictions of the global potential L. Fits with potentials F and F' are nearly identical. See Table II for a quantitative comparison with fits by other global prescriptions.

FIG. 5. Comparison of the 52-MeV data of Ref. 24 with curves from potential L. Curves from potentials F and F' are nearly identical. See Table II for comparison with other global prescriptions. For ^{103}Rh, ^{181}Ta, and ^{238}U low excited levels are included in the elastic peak and may distort the angular distributions at larger angles.

by refitting the $E = $const data sets at all energies, this time incorporating the polarization data from the beginning. The goal was to improve on all previous fits—admitting additional parameters if necessary. In this we retained our original criterion that additional (trial) parameters were kept only if they produced a χ^2 improvement above 10% for the total set. This last, but extensive search cycle resulted in potential F (for calculations with relativistic kinematics) and the very closely related potential L (for calculations with the nonrelativistic kinematics, which are used in most older DWBA codes). The newly introduced weak energy dependence in a_0 was essential for the significant improvement in fits over potentials A through E. The energy dependence in W (and in r_I for potential F) is somewhat less unique. The global potentials F and L are listed in Table III. The numerical χ^2 comparison with prior potentials is shown in Table II. A comparison of the predictions of potential L (in the nonrelativistic spin-1 formalism) with the experimental points of the full data set is shown in Figs. 2–8. The results of potential F would be visually almost indistinguishable from L and are not shown in the figures.
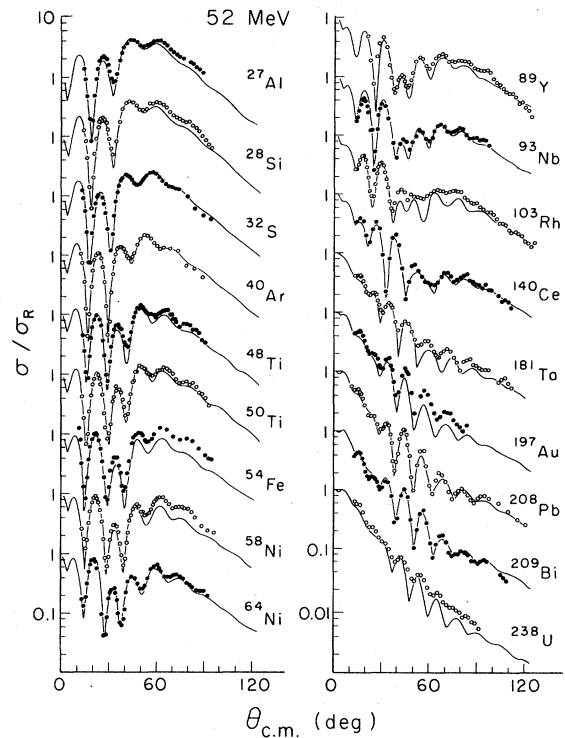
G. Unanswered questions concerning the reaction cross sections

Two comprehensive deuteron reaction cross section studies using attenuation techniques were performed at 22.4 MeV by Wilkens and Igo[57] and at 25 MeV by Mayo *et al.*[58] Predictions of potential L (which are very close to potentials $A-F$ at 25 MeV) are shown with the σ_R data in Fig. 8.

This section outlines our unsuccessful attempt to better fit the reaction cross section data. The lettered potentials $A-L$ give σ_R predictions for the lower energy (10–13 MeV) region which generally lie within the quoted experimental errors. (An exception is ^{12}C at 12.8 MeV, a very light target which we would not expect to fit well). However, a close look at the two surveys at 22.4 and 25 MeV indicates a systematic A dependence in the quality of fit. The predictions of potential L are good for low mass targets, but for the heavier masses there is a discrepancy between predictions and data, particularly with the 22.4-MeV data.

TABLE III. A listing of recommended global parameter prescriptions, which fit a wide range of deuteron scattering data. Potentials L and F are nearly equivalent in the range 15–85 MeV. Potential F' differs from F in having a complex spin-orbit term. The addition of the imaginary part (W_{LS}) provided a better fit primarily to polarization data. The F' parameters are tentative as only a small set of polarization data was available for this analysis. A = mass number, Z = proton number, $\beta = -(E/100)^2$, $\mu_i = [(M_i - N)/2]^2$, where M_i = magic numbers $(8, 20, 28, 50, 82, 126)$, N = neutron number, E = deuteron laboratory energy in MeV.

Potential name	V_R (MeV)	r_0 (fm)	a_0 (fm)	W_S (MeV)	W_D (MeV)	r_I (fm)
79 DCV, L (nonrelativistic kinematics only)	$88.5 - 0.26E$ $+0.88ZA^{-1/3}$	1.17	$0.709 + 0.0017E$	$(12.2 + 0.026E)(1 - e^\beta)$	$(12.2 + 0.026E)e^\beta$	1.325
79 DCV, F (for relativistic kinematics only)	$88.0 - 0.283E$ $+0.88ZA^{-1/3}$	1.17	$0.717 + 0.0012E$	$(12 + 0.031E)(1 - e^\beta)$	$(12 + 0.031E)e^\beta$	$1.376 - 0.01\sqrt{E}$
79 DCV, F' (for relativistic kinematics only)	$88.0 - 0.283E$ $+0.88ZA^{-1/3}$	1.17	$0.717 + 0.0012E$	$(12 + 0.031E)(1 - e^\beta)$	$(12 + 0.031E)e^\beta$	$1.376 - 0.01\sqrt{E}$
Example for ^{93}Nb F parameters at 52 MeV	81.25	1.17	0.7794	3.225	10.387	1.304

Potential name	a_I (fm)	r_C (fm)	V_{LS} (MeV)	r_{LS}	a_{LS}	W_{LS}	r_{ILS}	a_{ILS}
79 DCV, L (nonrelativistic kinematics only)	$0.53 + 0.07A^{1/3}$ $-0.04\sum_i e^{-\mu_i}$	1.30	$7.33 - 0.029E$	1.07	0.66	0	0	0
79 DCV, F (for relativistic kinematics only)	$0.52 + 0.07A^{1/3}$ $-0.04\sum_i e^{-\mu_i}$	1.30	$7.20 - 0.032E$	1.07	0.66	0	0	0
79 DCV, F' (for relativistic kinematics only)	$0.52 + 0.07A^{1/3}$ $-0.04\sum_i e^{-\mu_i}$	1.30	5.0	1.04	0.60	$0.37A^{1/3}$ $-0.03E$	0.80	0.25
Example for ^{93}Nb F parameters at 52 MeV	0.8223	1.30	5.744	1.07	0.66			

A data set was constructed of these two σ_R surveys, and searches were performed. By allowing only the non-structure-dependent terms of the imaginary diffuseness to vary, excellent fits ($\chi^2 \lesssim 1$) to σ_R were obtained with $a_I = 0.65$ fm. This value is to be compared with the potential L value of $0.53 + 0.07A^{1/3}$ fm, which would yield $a_I = 0.74$ to 0.95 fm for a typical target range of Al to Pb.

Thus the reaction cross section fits seemed to suggest that there should be no residual mass dependence in the imaginary diffuseness a_I, and in addition that the overall magnitude of a_I is too high. As a result, attempts were made to revamp the global potential to exclude the mass term in the imaginary diffuseness. This necessitated a steeper mass dependence of the real potential depth and also the inclusion of a mass dependent term in the real diffuseness a_0. The resulting potential we called potential T.[52] The advantage of potential T was that without the A dependence in the absorptive potential, the changes in the

σ_R predictions with A reflected the changes of the 22- and 25-MeV σ_R data. Also, we observed that the differential cross section predictions for heavy targets $(A > 200)$ at the low energies $(E \leq 17$ MeV) displayed more structure than potential L.

The disadvantages of potential T, however, greatly outweigh the advantages. First, although potential T fits the change in σ_R with A quite well, the magnitude of the imaginary diffuseness a_I required to fit the differential cross section data (0.82 fm) still yields too much absorption *overall* for the σ_R data. Searches on the differential cross section data using potential T with a_I fixed at 0.65 fm generates fits whose total χ^2 is eight times larger than with a_I of 0.82 fm. Consequently, even potential T overpredicts the 25-MeV σ_R data by 12% and the 22-MeV σ_R data by 20%. Secondly, potential T predicts too much structure in the heavier targets $(A > 100)$ at 52 MeV, in a few cases, predicting oscillations not reflected at all in the data. Finally, the most
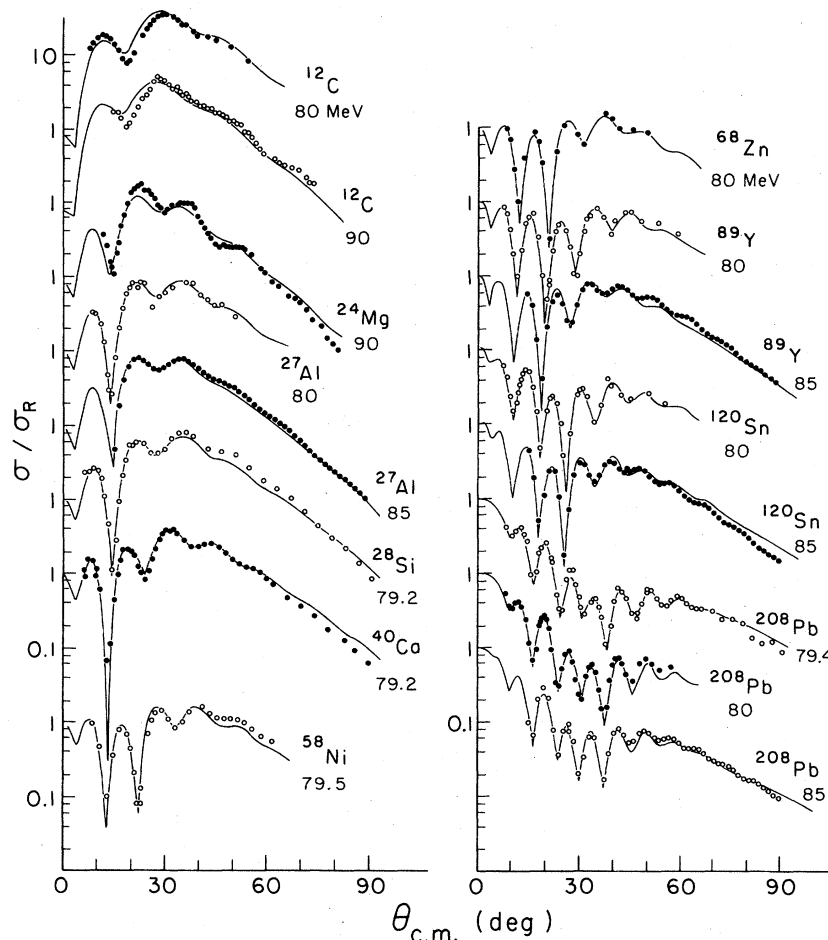
FIG. 6. Comparison of 80–90-MeV data (Refs. 39–42) with curves from potential L. Fits with potentials F and F' are marginally better. The other global prescriptions are not very useful at this energy. (Compare Table II.) It is noted that the data for 79.2 and 79.5 MeV (Ref. 42) are tentative and subject to small changes.

significant objection to potential T is the quality of its polarization predictions. The central part of potential T distorts the polarization predictions qualitatively to such an extent that it is impossible to obtain good fits with *any* values of the spin-orbit parameters.

Finally, we explored the effect of a possible asymmetry in the surface of the real potential. The folding computation of the real deuteron optical potential by Perey and Satchler[2] yielded a related local potential with a near Woods-Saxon form if the diffuseness was made asymmetric about the half-radius point. The effective folded real Woods-Saxon form would then have a typical inner diffuseness of $a = 0.68$ fm and an outer (tail) diffuseness of 0.82 fm varying slowly with A. This could in turn be represented by an A-dependent term in a_0. That is, for a given bombarding energy, the incident deuteron would see more of the tail region of a heavier target, where the folding model predicts a large diffuseness. An

attempt was made to employ this asymmetric a_0 term with our data in GENOA, with hopes that it might replace the need for an $A^{1/3}$ dependence in the σ_R global potential. After a number of searches, the resulting fits were about 10% worse, with the two diffuseness values (a_{in} and a_{out}) tending to converge to one another. It has not yet been possible to use such an asymmetric a_0 to obtain the overall goodness of fit we ordinarily obtain, without a major reorganization of the real potential.

The failure to accurately reproduce an appreciable fraction of the total reaction cross section data is of concern. It could imply that in the global prescriptions some important phase shifts are not obtained correctly. Hence we expended considerable effort trying to overcome this difficulty, as outlined above. Our present feeling is that even individual best-fit parameters for 22.4-MeV angular distributions (if available) would give total cross sections larger than the
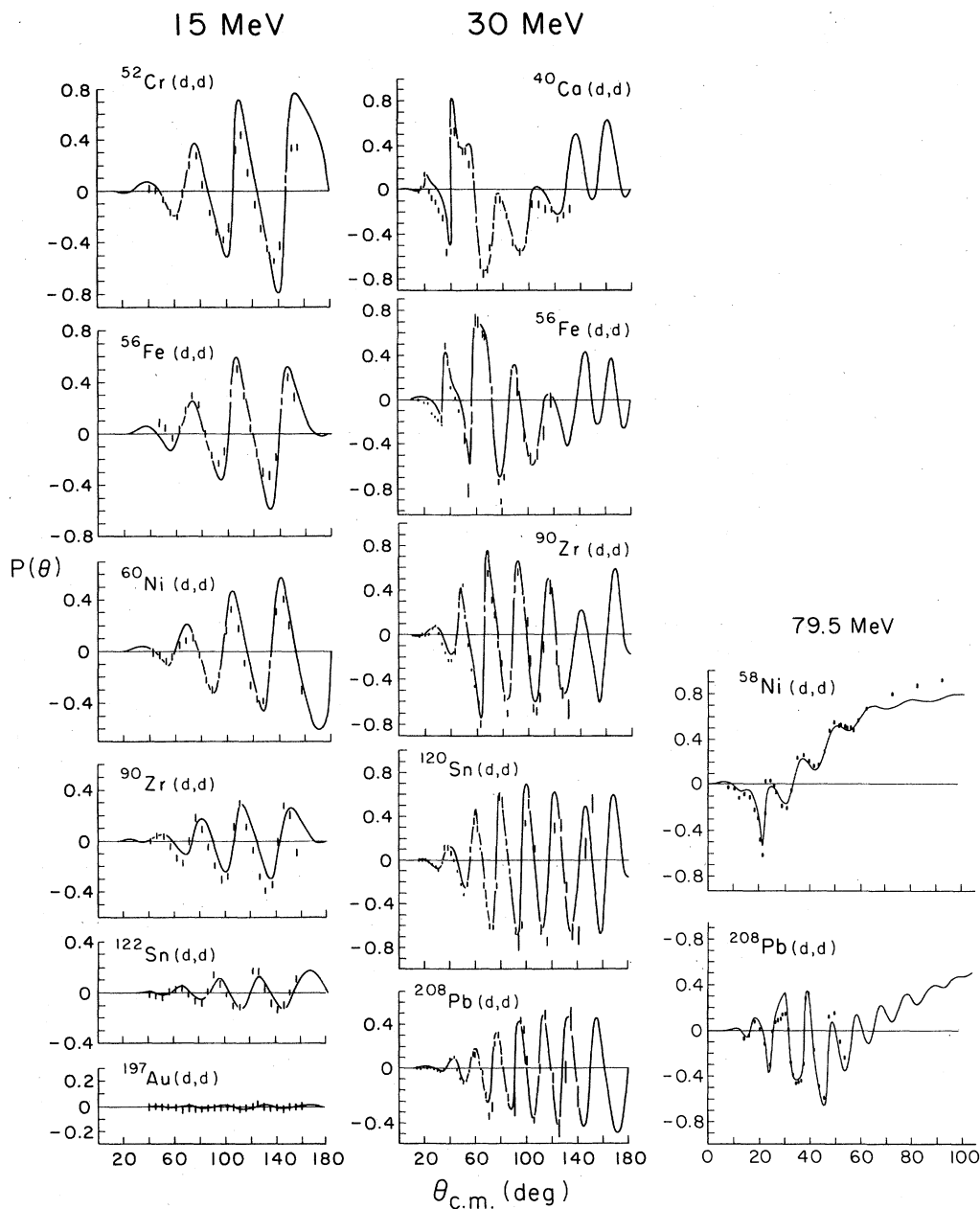
FIG. 7. Comparison of potential L predictions with vector polarization data from Refs. 54, 55, and 42. The 79.5 MeV polarizations (Ref. 42) are preliminary. Fits with potential F are marginally better, while potential F' (by virtue of the complex spin-orbit term) does noticeably better. See text and Tables II and III.

measured ones. We refer to Fig. 22 in Ref. 17(a) where best-fit parameters for 21.6-MeV angular distributions are used to predict total cross sections. These (21.6-MeV) reaction cross section predictions are about 10% larger than the measured ones at 22.4 MeV. Figure 9 shows the predictions of potential L for σ_R as function of A and E. It can be seen that, for targets with $A \geq 100$,

σ_R grows very rapidly with E, i.e., by about 4% per MeV in the 20-MeV region. Accounting for this trend further increases the disagreement already apparent in Perey's best-fit comparison.[17] We thus may see a limitation of the optical model analysis for deuteron scattering. On the other hand, such a conclusion should probably be deferred until these early and difficult measure-
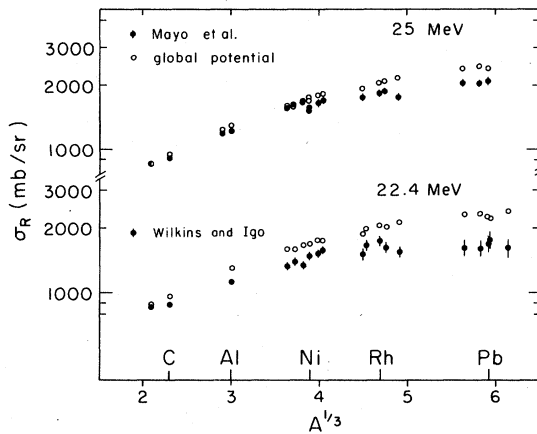
FIG. 8. Comparison of the reaction cross section data of Refs. 57 and 58 with the predictions of potential L. The low-energy data (not shown) and the data for small A give good agreement with the optical model predictions of potentials $A-L$. However, for the heavier targets all predictions are systematically higher than the data shown, particularly for 22.4 MeV. Forcing a fit to these reaction data produces dramatically inferior fits to the polarization data.

ments have been checked with improved experimental methods.

III. DISCUSSION

A. Comparison with experimental data

In some respects the highest energy data (80–90 MeV) should be hardest to fit. There are more and generally deeper minima than at lower energies, and the rapid variation with θ would present problems if measurements are uncertain by as little as 0.5°. However, a glance at Fig. 6 shows that the global approach leads to very satisfactory fits. Some cases of excellent agreement are found at all energies investigated (Figs. 2–7), but we also notice a number of disagreements. Most of them, we feel, can be under-
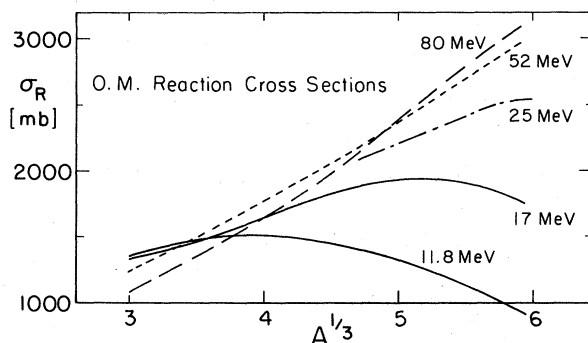

FIG. 9. Predictions of potential L for the mass and energy dependence of the total reaction cross sections.

stood for the reasons given below.

(a) All but the most recent experiments used deuteron beams of moderate resolution (i.e., >100 keV), and a number of the experimental cross sections are, therefore, suspect at large angles. For instance, the measured cross sections for ^{93}Nb, ^{103}Rh, ^{181}Ta, and ^{238}U contain the inelastic cross section for one or more unresolved states below 150 keV excitation. Inelastic contributions are generally out of phase and wash out the elastic structure. The angular distributions which we suspect on experimental grounds are noted in the figures. They generally lie *above* the calculated curves, as might be expected. This is especially obvious for ^{218}U at 52 MeV (Fig. 5).

(b) The cross sections for the lightest targets at 11.8 and 17 MeV show systematic disagreements with the optical model curves $[\sigma(\theta)_{exp} - \sigma(\theta)_{theor} \simeq$ const for low E, A, as for protons[22]]. We think this effect is meaningful and not an artifice of the data or the analysis. Its disappearance at higher energies suggests that compound-elastic scattering and/or other higher order effects are not negligible, at 11.8 and 17 MeV. The optical model is not expected to work well when such effects are important.

(c) At 11.8, 17.0, and 34.0 MeV data for $f_{7/2}$ targets show recurring differences from the calculated curves. This could be a more subtle structure effect which the optical model in its current form cannot predict (e.g., a nonuniform increase of R with A). This effect is particularly striking for ^{48}Ca in Fig. 3. $\sigma(\theta)$ for ^{48}Ca shows almost no similarity to that of the neighboring ^{51}V, which also has a closed ($N=28$) neutron shell. In most other atypical, shell-closure correlated variations the global fits were improved considerably by the introduction of the magic shell correction term for a_I. Minor problems at large angles remain. See, for instance, $\theta > 150°$ for ^{89}Y, ^{93}Nb, ^{124}Sn, and ^{208}Pb in Fig. 3. A 50% larger magic term would better reproduce these shell effects at 17 and 34 MeV; however, it would harm the fits at higher energies. The coefficient of 0.04 given in Table III represents a compromise.

(d) A few angular distributions (e.g., ^{54}Fe and ^{197}Au at 52 MeV) disagree with our global fits by being systematically 30–50% higher everywhere, even at very small angles (Fig. 5). It is our experience that such disagreements often result from an incorrect normalization of the data. (We noted in our own measurements that ^{197}Au absolute cross sections could not be reproduced from run to run because of the nonuniformity of our commercial self-supporting

gold foils). A remeasurement for ^{54}Fe and ^{197}Au would be very desirable.

B. The real potential

The historically observed discrete ambiguities for the depth V_0 of the real potential[16,17] have essentially been resolved by the folding method[1-3,5] in favor of a potential characterized by a volume integral $J/2A \approx 350$ MeV fm^3. As explained above, this theoretical result was one of the boundary conditions imposed on our searches. But the familiar continuous ambiguity for r and V_R characterized by the empirical relation $Vr^n = $ const was not resolved when this study began. Owing to the ability of empirical models to fit proton-nucleus scattering with radius parameters ranging from 1.15 to 1.25 fm (Refs. 21, 22, and 20), a range of $1.1 < r_0 < 1.2$ for the deuteron-nucleus radius parameter is consistent with the folding approach. The analysis of the lower energy data showed no striking preference for any particular r_0 value inside this range; however, by and large, the lowest energies were more easily fit for $1.1 \leqslant r_0 \leqslant 1.15$ and the highest ones (80–90 MeV) were better fit with $1.15 \leqslant r_0 \leqslant 1.20$. We have somewhat arbitrarily resolved this ambiguity by demanding that r_0 should not be energy dependent. There is no clear theoretical guide as yet on how r_0 should change with E, and $r_0 = $ const is the simplest and a palatable option. It was found that for $r_0 = 1.17$ fm, high and low energy data could be well fit as long as a small energy dependence of a_0 was permitted. (a_0 for potential L grows linearly from 0.73 fm at 12 MeV to 0.825 fm at 90 MeV.) This energy dependence of a_0 is no longer optional if r_0 is kept at a (any) constant value. We see no unusual significance in this particular parametrization except that it works and involves reasonable values for r_0 and a_0. We note that R_{rms}, the resulting rms radius for the potential, is apparently unique for potentials of the Woods-Saxon shape and should be reproduced by a successful theoretical construction of the real potential. Figure 10 shows the values $R_{\mathrm{rms}}(E)$ for several nuclei as predicted by potential L. A moderate but distinct increase in R_{rms} with energy is seen. This trend is supported quantitatively by independent, individual best-fit rms values which were taken (mostly) from the literature and are shown as circles in Fig. 10. The agreement of best-fit rms values with the global potential L is better than expected given the usual fitting ambiguities.

In Fig. 11 we show as solid lines the real volume integrals $J/2A$ extracted by our global fit. Again the circles are independent best-fit values. The value of $J/2A$, at least if obtained
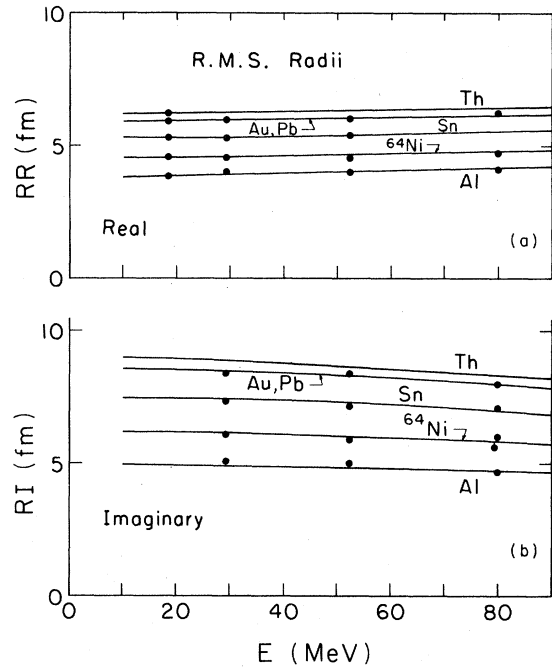

FIG. 10. The solid lines represent rms radii extracted from the global analysis of our data set. They were computed from potential L for several targets as a function of energy. We note the close agreement with corresponding real and imaginary rms radii extracted in the literature from individual best-fit analyses (e.g., Refs. 38, 26, 24, 39, and 42, shown as closed circles).
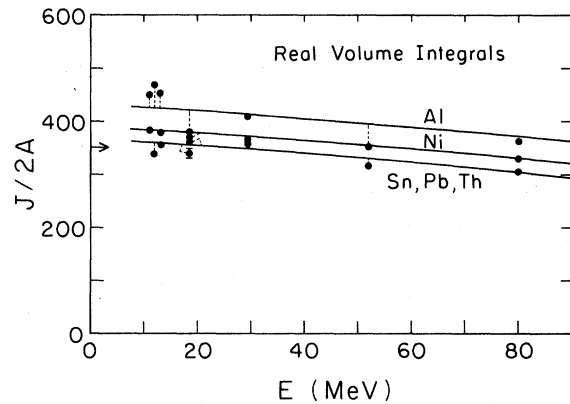

FIG. 11. The solid lines show the energy dependence of the real volume integrals for several targets as extracted by the global fit L to our data base. Corresponding volume integrals ($J/2A$) deduced from best-fit parameters in the literature (full circles) agree with these lines to about 10% or better. We noticed that $J/2A$ depended somewhat on the r_0 values chosen in the optical model analyses. The real volume integrals decrease almost linearly with energy and show a nonlinear dependence on A.

from individual best fits, seems to be less unique and more strongly dependent on the choice of the real radius parameter. Note the large scatter at 11–17 and at 52 MeV around the "global" curves. The 52-MeV points result from ($r_0 = 1.05$) best fits.[24] We believe that so small an r_0 value is unphysical at 52 MeV. The lower energy best fits use more conventional r_0 values, but do not seem to determine $J/2A$ very precisely. Our global fit indicates a distinct, nearly linear drop of $J/2A$ with energy, a feature that is also seen in proton scattering and thus expected, at least qualitatively, from folding theory.

$V(r)$ of potential L has been carefully optimized for the available data set. Given the number of variables used and potential shapes of Woods-Saxon type we find the parametrization of Table III superior to all others we have tried. This is not to say that better shapes could not be found. Even if we retain $f(r)$ some ambiguities persist. Using the notation $V_R(r) = (V_0 + K_1 Z A^{-1/3} + K_2 E) f(r)$, they can be expressed roughly by the relation $V_0 + 9K_1 = C = $const, where the constant C depends on the fixed real radius value r_0. Quite good fits could be maintained with ±20% variations in K_1 as long as the above relationship was satisfied. It is interesting to note that for Perey's[17] set B ($V_0 \approx 100$ MeV, $r_0 = 1.15$), $K_1 = 2.0$ and $V_0 = 81$, so that the constant $C = 99$ MeV. The global potential E ($V_0 = 89.5$ MeV, $K_1 = 1.0$) has $C = 98.5$ MeV. For our potential L ($r_0 = 1.17$, $V_0 = 88.5$ MeV, $K_1 = 0.88$) we have $C = 96.4$. Hence the divergent values for K_1 appear to be part of a long valley in χ^2 hyperspace.

The Coulomb term was originally introduced into the optical model potential in the proton studies by Perey[21] and by Becchetti and Greenlees[22] to represent an energy correction term to the real potential depth. Thus, a deuteron will experience a Coulomb repulsion of about $1.38 Z / A^{1/3}$ MeV at the nuclear surface. Since our energy dependence is $0.28E$ we might then expect a net energy correction of $0.28(E - 1.38 Z / A^{1/3})$ $= 0.28E - 0.39 Z / A^{1/3}$. The fitted value of $0.88 Z / A^{1/3}$, being more than twice the expected value, could probably not be explained away by corrections to the Coulomb term. It appears rather that the "Coulomb" term in V_R represents actually two separate terms, the first being a contribution due entirely to Coulomb repulsion, and the second being an A-dependent fitting parameter. In fact the $Z / A^{1/3}$ term may be a disguised term of the form $A^{2/3}$, which behaves very similarly with A for most targets. Even our previously observed ambiguity between V_0 and $K_1 Z / A^{1/3}$ does not extend down to the region of $0.4 Z / A^{1/3}$ without considerable worsening of the fits.

The energy dependence of V_R is well defined for a given r_0. Whenever the potential depth V_R was plotted versus energy for best fits for a single isotope at various energies with a common real geometry, a very nearly straight line was described by the points, up to 52 MeV. Thereafter, the slope increased somewhat. It is expected that outside the incident deuteron energy range of 11.8 to 85 MeV, such a linear approximation for $V_R(E)$ would not hold. The energy dependence of V_R for nucleons should become weaker as E increases further.[59] However, for the energy range we analyzed, a linear dependence was adequate and it was not deemed advisable to employ a more complicated E dependence.

The real radius parameter r_0 was fixed to a given value for most fits performed, both single and global. Attempts were made to introduce a radius of the form $r_d + r_0 A^{1/3}$ where $r_0 A^{1/3}$ would be the nuclear radius and r_d would represent the deutron size. However, fitting with such an expression brought no improvement and the addition of such a term seemed thus unjustified. At various times the radius was allowed to go free for each target in a global fit, but no systematic variance from a constant value could be detected.

The real diffuseness a_0 was observed to be tied to the real radius, in an inverse relationship. Freeing a_0 with fixed r_0 on targets in a global fit showed a slight energy dependence. This E dependence of a_0 was found to be easily absorbed by the E dependence of the real depth V_R unless and until the 85-MeV data were included.

In general, the global fits over broad mass ranges required an A-dependent term in one of the central diffuseness parameters—in a_0 or in a_I. Putting the A dependence in a_0 rather than a_I, while improving the overall slope of the σ_R fits with mass, considerably worsened the differential cross section fits overall.

C. The imaginary potential

The simple Watanabe model[1] is not adequate for a correct prediction of the imaginary part of the optical potential.[2,3] This is mostly due to the large probability of deuteron breakup in the scattering process.[3,5,7] Extensive theoretical work in recent years[8,12,13,15] has greatly enhanced understanding of this process. The simple folding of imaginary nucleon-nucleus potentials considerably underpredicts the imaginary potential needed, and breakup is a major physical cause for the large imaginary surface term found in the phenomenological deuteron-nucleus potential.[15] The processes contributing to the absorption of the incident deuteron wave are sufficiently com-

plex as to discourage a quantitative construction of a local, equivalent optical model term. Hence most recent theoretical calculations for deuteron scattering compute the scattering matrix elements directly. When a comparison with the matrix elements obtained from the optical model is made it is noted that theoretical refinements tend to give matrix elements which more closely agree with phenomenological values.[8]

Qualitatively, it is expected that as the deuteron energy increases, the absorption will decrease at the surface and increase in the volume region of the target.[18] Such a dependence was also found empirically by Becchetti and Greenlees[22] in their elastic nucleon optical model studies. For protons, Becchetti and Greenlees obtained $W_S = 0.22(E - 12.3)$ and $W_D = 11.8 - 0.25E$ +(isospin term), i.e., the surface potential drops to 50% of its maximum value at 24 MeV per nucleon. This is about twice as steep a drop as found for our deuteron potentials A to E which employ a similar parametrization. This linear energy dependence did not work so well once the data set was extended to 90 MeV. The fits to the 85-MeV data indicated a preference for a stronger switch to an imaginary volume potential than given by potential E. The very slow drop of W_D at low energies and the faster drop at and beyond 52 MeV, which we found empirically, could be approximated by a Gaussian function of the type $W \exp[-(E/E_0)^2]$. This function also has the advantage that it will not cross zero (as any linearly decreasing function would). The least squares search fixed E_0 at 100 MeV to within about 10% (depending on geometric parameters). Hence our imaginary potentials took the form

$$W_D = W_1(E) \exp[-(E/100)^2],$$

$$W_S = W_2(E)\{1 - \exp[-(E/100)^2]\},$$

where $W_1(E)$ and $W_2(E)$ showed a very weak increase with E. It was found that for all practical purposes we could set

$$W_1 = W_2 = W = 12.0 + 0.03E$$

and

$$W_D = W - W_S.$$

In this parametrization, W_D drops to 50% of its maximum at 40 MeV per nucleon, or at 80-MeV deuteron energy, faster than for the low energy potential E (which yields the half point at $E_d = 113$ MeV), but not as fast as the Becchetti-Greenlees potential for protons (which would have yielded the half point at 48-MeV deuteron energy). The Gaussian shape in our parametrization is somewhat arbitrary, but there is reasonable (χ^2)

evidence for the nonlinearity in the decrease of W_D and the corresponding nonlinear increase of W_S.

The strong coupling of W_D and W_S is a consequence of the near constancy of the imaginary volume integral which is demanded by the data. Figure 12 shows the volume integrals $JI/2A$ deduced from our global fit L as function of deuteron energy. The upper five curves refer to targets of different sizes and give the total imaginary volume integrals. The lower two curves give the surface (JD) and volume (JS) components separately for ^{124}Sn. The circles represent independent best-fit results from the literature. They are connected by vertical lines to the curve to which they correspond most closely in mass $(\Delta A = \pm 2)$. These best fit values scatter about the global curves, differing by 5 to 10%. They do, however, agree well with our global fit conclusion that the total imaginary volume integral per nucleon is nearly constant with energy and decreases with target mass. There is as yet no independent test for the magnitude of the volume
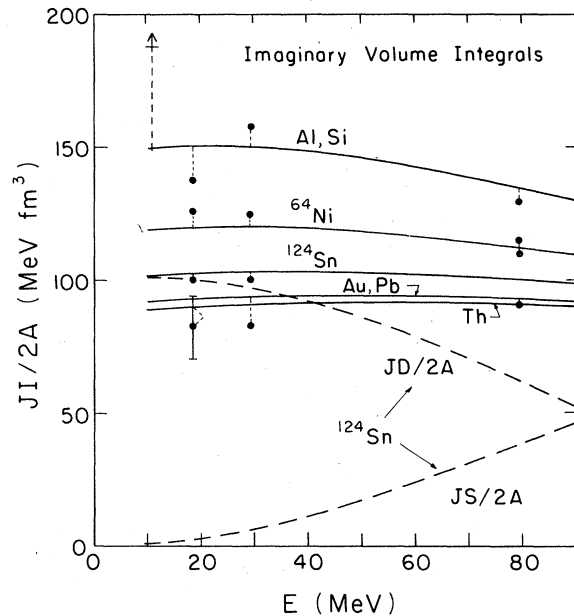

FIG. 12. Lines show imaginary volume integrals $(JI/2A)$ deduced from the data through the global fit L. Corresponding individual best-fit values for $JI/2A$ are taken from the literature and shown as closed circles. Above 15 MeV deuteron energy agreement to within 10% is seen; however, individual best fit values reported at 11 MeV (arrow) disagree by 30% or more. It is noted that $JI/2A$ varies strongly with A, but only very gradually with energy. The dashed lines separately show the changing surface $(JD/2A)$ and volume $(JS/2A)$ components of the integral for ^{124}Sn. Both parts contribute about equally at 90 MeV.

and surface parts separately. The arrow at 11
MeV is added as a reminder that the volume inte-
grals for <12-MeV best fits[6] are not close to our
global curves, being much larger than at higher
energy and showing larger scatter.

A glance at Fig. 10(b) shows that our global
parameters and the independent best-fit param-
eters from others deduce remarkably similar
imaginary rms radii RI_{rms}, in spite of the fact
that other analyses use rather different r_I, a_I
parametrizations. Hence, good fits to the data
over a sufficiently large angular range apparent-
ly fix the real and imaginary root mean square
radii of the scattering potentials rather accurate-
ly (in contradistinction to the continuous am-
biguities in the optical model parameters r_0
and r_I). The global and individual best-fit analy-
ses agree that RI_{rms} for a given target *falls* slowly
with deuteron energy and can be considered well
known.

We return briefly to the question of volume
versus surface absorption components. Figure
13 shows the radial dependence of the combined
imaginary potential contributions as given by the
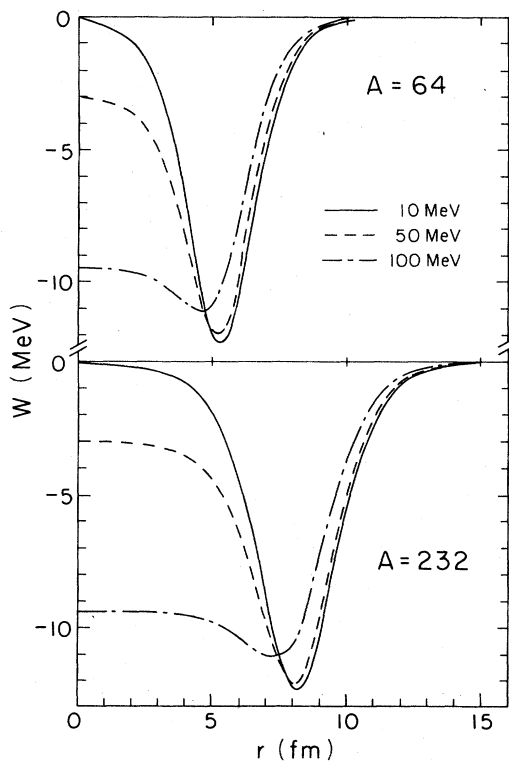global potential L for two nuclei of very different

FIG. 13. Radial dependence of the imaginary parts of
the optical potential L as a function of deuteron energy
for two targets. Note that the half-value radius is mark-
edly affected by the shift from surface to volume ab-
sorption without a change in the radius parameter r_i.

size. We note that the switch from surface to
volume dominance automatically reduces the
half point radius with increasing energy. This
decrease of RI is a real effect needed to fit the
data well. However, the magnitude of W at
$r \approx 0$ is probably not well determined by our data.
It is determined only in the following sense:
Throughout our global fitting study we followed
the self-imposed rule that the *minimum* require-
ment for the introduction of a new parameter is
the improvement by 10% in χ^2 for the data set.
It was known that lower energy data (~17 MeV)
required no appreciable volume term but did
need a surface term with $r_I \approx 1.33$. On the other
hand, medium energy proton $E > 50$ and higher
energy deuteron data have been fit best with a
volume absorptive potential. Similarly, nucleon-
nucleus folding calculations predict increased
volume absorption at higher energy.[18] This led
us to introduce both potential shapes. Given this
additional complexity we subsequently tried to
not further increase the parameter space by
holding r_I and a_I to the same values at all energies
and for both radial shapes. This constraint led
to W_D and W_S values which were well fit by the
Gaussian energy dependence given above. It
came as a pleasant surprise that the best fits
resulted in $W_1 \approx W_2$, thus eliminating the need for
one of the W parameters. There are undoubtedly
other and more complex $W(r, E)$ parametriza-
tions which would fit the data equally well or
better.

For the range of our fits $W = 12.0 + 0.03E$, i.e.,
W grows slowly but linearly. This probably
cannot be extrapolated very far beyond 100 MeV.
Generally, we expect that at higher energies
optical parameter energy dependences will be-
come weaker, with the imaginary depths asymp-
totically approaching a constant value. Such be-
havior has been observed with elastic nucleon
scattering, where W_S rises with increasing
bombarding energy from a depth of 5 MeV to a
depth of 20 MeV (at 50-MeV incident energy) (Ref.
59, p. 175, see also Ref. 20), but for incident
energies from 50 through 300 MeV, W_S remains
fairly constant.

The imaginary radius parameter r_I is fairly
stable in the region 1.30–1.33 fm with our global
fits, showing a preference for the lower value
at the higher energies. $A^{-1/3}$ terms were intro-
duced into r_I at various times, but no particular
advantage was obtained. The imaginary diffuse-
ness a_I is the parameter which we have chosen
to contain the observed structure dependence.
The shell correction term which is a function of
closed neutron shells reduces absorption by
making the imaginary diffuseness sharper near

and at magic neutron numbers. Although a great deal of scatter was seen in plots of best a_I versus nearness to magic neutron shell, the distribution $a_I(N)$ could be fitted quite adequately with a Gaussian centered at the magic shell number with a half-width of about 2.0 neutron numbers. This variation of a_I has a striking resemblance to the drop of the average level spacings near and at shell closure,[60] and is, conceivably, a consequence of it.

D. The spin-orbit potential

Knutsen found that the adiabatic folding $L \cdot S$ potential is well approximated by an effective spin-orbit potential of the Thomas form with a depth of 5.63 MeV and a geometry of $r_{LS} = 0.98$, $a_{LS} = 1.00$ fm.[61] Our initial global fits (potentials A, B, and C) were performed with this geometry. Initially, we varied only the spin-orbit depth. Later, searching on the 15-, 30-, and 80-MeV vector polarization data, the spin-orbit geometry as well as the depth was allowed to vary. The data at the higher energies showed a definite preference for a much narrower diffuseness ($a_{LS} = 0.55$ fm), with roughly the same depth and radius ($V_{LS} = 5.5$ MeV, $r_{LS} \approx 1.0$ fm) as the folding results. The fits were somewhat insensitive to changes in the radius r_{LS}. However, they were very sensitive to changes in the diffuseness, and the final fits with the narrow values of 0.55 to 0.66 give about half the χ^2 of the fits with the fixed folding geometry.

For the 15-MeV data the advantage of the narrower spin-orbit diffuseness ($a_{LS} = 0.55$ fm) was less visible in our analysis because the major errors arose from a phase shift between data and calculation (see Fig. 7). At 15 MeV the $P(\theta)$ curves have crossover points about 3° farther back than the data. This is not influenced much by the value of a_{LS}. This problem has been encountered before for individual fits at this and lower energies.[6,62] Goddard and Haeberli suggested that the introduction of a small imaginary spin-orbit term can remove this phase shift and also improve the fit to the tensor analyzing powers.[62] They gave five examples each at 10 and 15 MeV where a best-fit search with a complex spin-orbit potential (six free spin-orbit parameters per nucleus) gives good fits for vector and tensor polarizations, whereas omitting the imaginary spin-orbit terms increases the best possible χ^2 by about 70%. Similar conclusions have been drawn by Bürgi et al.[43] from an analysis of 9–12-MeV polarization data for ^{40}Ar. Both analyses use very narrow spin-orbit geometries, i.e., $r_{LS} \lesssim 0.8$, $a_{LS} \leqslant 0.50$ for the real part and $0.7 \lesssim R_{ILS} \leqslant 1.1$, $0.2 \lesssim a_{ILS} \leqslant 0.35$ for the

imaginary part, but such extremely narrow geometries have not been found in folding studies. More recently Quin[63] has reported that similar problems for polarization data at low deuteron energy could be remedied by taking explicit account of some large stripping channels in a coupled channel analysis. Quin's approach appears promising; however, it falls outside the scope of this study.

We note that generally, but particularly at 15 MeV, *simultaneous* good fits to cross section and polarization data are difficult to obtain with just a real spin-orbit term, even if only individual targets are fit. The systematic differences between data and calculations visible in Fig. 7 and in a different perspective in Fig. 14 seem less the result of our reliance on a global parameter prescription than of a shortcoming in the (real) polarization term given in the Introduction. Although we have no theoretical guidance for the exact form of a complex spin-orbit term, the existence of a weak imaginary component is suggested by folding considerations[5] and a recent proton scattering analysis.[20] Hence we let the spin-orbit term become complex in some of our global searches. Initially the real and imaginary terms had the same geometry: $V_{LS}f(r)$ $\rightarrow (V_{LS} + iW_{LS})f(r, r_{LS}, a_{LS})$. The results of such searches were negative. W_{LS} did not converge to any particular value and the fits were not appreciably improved. In our recent searches we permitted different geometries for the real and imaginary parts, i.e., $V_{so} = V_{LS}f(r, r_{LS}, a_{LS}) + iW_{LS}f(r, r_{ILS}, a_{ILS})$. It was found that $a_{LS} \gg a_{ILS}$
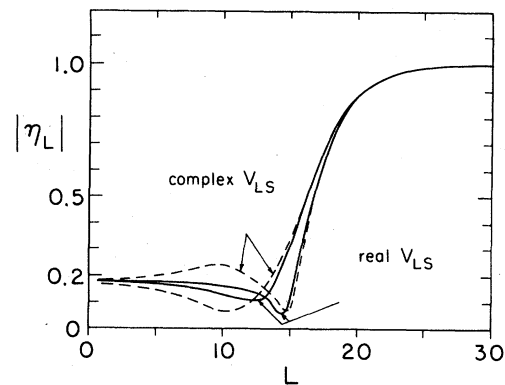

FIG. 14. Plot of S-matrix moduli η_L as a function of L for fits to ^{58}Ni at 79.5 MeV. The solid lines are derived from the global potential F. They are very similar to those from potential L and represent phase shifts for the highest and lowest couplings of $\vec{L} + \vec{1}$, respectively. The addition of an imaginary spin-orbit term in potential F' improves primarily the polarization fit, but leads to considerable changes in the phase shifts for the lower partial waves ($L \leqslant 12$).

≈ 0.25, for superior fits. Also, W_{LS} proved energy dependent and changed sign between 30 and 70 MeV. A comparison of polarization data with such an extended potential is shown in Fig. 15. The very limited number of high energy polarization measurements in our data set makes it difficult to draw firm conclusions about the imaginary spin-orbit term. However, a trial potential with a complex $L \cdot S$ term is listed in Table III as prescription F'. Further work is clearly warranted and is contemplated in connection with new measurements of vector and tensor polarizations at the Indiana cyclotron.

The results of this study support making V_{LS} energy dependent. A reduction of V_{LS} relative to the low energy data was necessary at 80 MeV. A decreasing $V_{LS}(E)$ also provided significant improvements for the vector polarizations at 30 MeV. The linear relation $V_{LS} = 7.33 - 0.029E$ of potential L is adequate, but not unique in the 12–90-MeV range. The value $a_{LS} = 0.66$ is an uncertain compromise. If greater weight were given to the elastic scattering cross sections, its value would go up by about 0.1 fm. Conversely, a much heavier weighting of the vector polarization would reduce a_{LS}. The parameter $r_{LS} = 1.07$ similarly is only certain to about 0.15 fm, the reason being the differing preferences shown by polarization and (high energy) scattering data. All in all the spin-orbit parameters are the least well determined ones in our set. Changes up or down from the average values given affect different parts of the data set in opposite ways.

We tentatively conclude that these uncertainties reflect not only the scarcity of polarization data at higher energies, but possibly the inadequacy of the functional dependence of the spin-orbit term and of the imaginary central potential as traditionally used. Although not yet warranted by our $\gtrsim 10\%$/parameter rule, a potential like potential F' may be justified as more polarization data are used in the data base.

It may be worth emphasizing that the strength of spin-orbit potential V_{LS} strongly affects the large angle ($\theta > 45°$) range of the 80–90-MeV scattering data and acts as a sensitive fitting parameter at the higher energies. This can be understood from Fig. 14 which shows the [58]Ni phase shifts η_L for $J = L \pm 1$ couplings of the spin-1 projectile. Scattering and absorption for the surface waves is seen to depend strongly on J, even in the absence of an imaginary spin-orbit term. The strong J dependence of the phase shift may also determine the onset of the loss of structure in the angular distributions.

Similarly, the different absorption of the ($J = L \pm 1$) partial waves in Fig. 14 for different
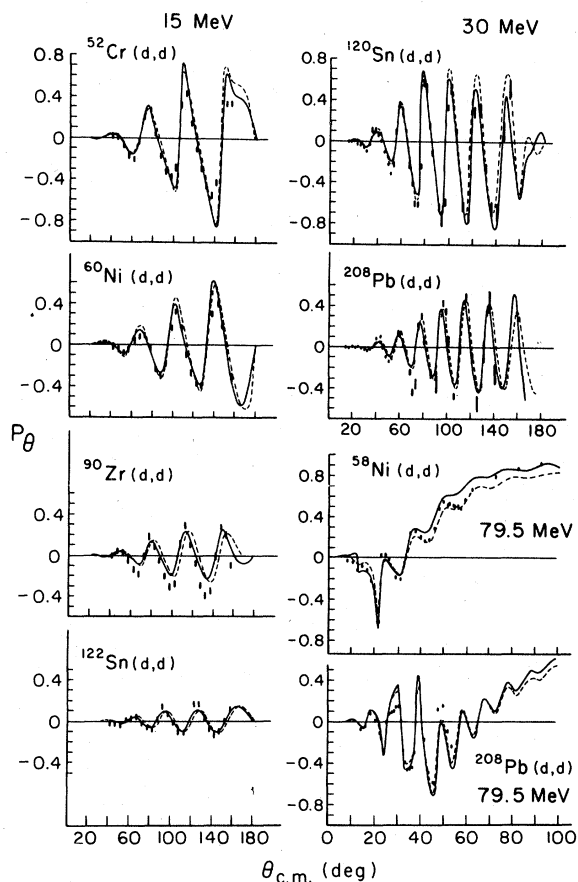

FIG. 15. The less adequately reproduced polarization data of Fig. 7 are shown here in comparison with predictions of potentials F and F' of Table III. Potential F curves are shown as dashed lines. Although not identical with those of potential L in Fig. 7, they are of similar quality and show similar shortcomings, as was seen in a detailed comparison of χ^2 values ($\chi_L^2 \approx \chi_F^2 \approx 7.4$). The use of a complex spin-orbit potential (global prescription F') results in the calculated vector polarizations shown by the solid lines. χ_{av}^2 for these curves is improved by a factor 0.7. The greatest changes are seen at 15 MeV. The imaginary term W_{LS} needed for better fits changes considerably and systematically with target mass and deuteron energy. The W_{LS} values for 15 MeV are close to those of Ref. 62. However, at 30 MeV W_{LS} is very small and has changed sign at 79.5 MeV. Note that the visible effects also change with energy. At 15 MeV predictions are shifted toward smaller angles, often by as much as 3°. At 30 MeV a similar but smaller shift is seen, whereas at 79.5 MeV the main effect is a 10–20% enhancement of the polarization at larger angles.

deuteron spin orientation may be responsible for the observation at 80 MeV of a large polarization of the same (positive) sign for all angles past 40°. A complex spin-orbit term enhances this

effect, through its influence on smaller L partial waves (see dotted lines in Fig. 14).

IV. CONCLUSIONS

Experience has shown that average optical parameter or "global potential" prescriptions tend to be successful within the mass and energy range of the data bases from which they were derived. Extrapolation to lower energies was quite successful for the Hinterberger[24] and Perrin[26] prescriptions, but all of the tested potentials were surprisingly unsuccessful when extrapolated into a higher energy range. Although noticeably better than the published global potentials, our early prescriptions named A through E,[52] which were derived without the consideration of data above 52 MeV, also lose a lot of their predictive power when extrapolated to 80 MeV (compare Table II).

The comparison of Table II suggests that our most recent potentials F and L are equal or superior to the others tested over the 12–90-MeV range, but there is a continuing lack of detailed theoretical guidance. Therefore, significant extrapolations, e.g., to energies above 100 MeV, probably would be of a quality just as uncertain as that which has been found for extrapolations of earlier sets.

It seems on theoretical grounds that the linear energy dependence given for V_R and $W(E)$ (Table III) is too simple; however, no quantitative theoretical estimate for the local equivalence of a current folding potential has been available. It is also unlikely that a_0 and V_{LS} should retain their linear energy dependence over a wide energy range. The linearity of most correction terms in Table III merely reflects the fact that the relatively weak energy dependences that were found could be determined only to first order. On the other hand, it is encouraging that the global prescriptions L and F are useful *and* remain simple for an energy range from 12 MeV to seven times that value.

As in most preceding studies the predictions at 11.8 MeV (Fig. 2) are poor for the light targets. (We note again that these targets deliberately were weighted less in the data sets.) The complicated behavior of the polarizations and the enhanced cross sections for backward angles at the lower energies seem to indicate that compound or higher order direct effects like coupled stripping channels make important contributions. We also noted a problem with the ^{27}Al and ^{48}Ca angular distributions at 17 MeV.

Aside from the exceptions mentioned above, satisfactory global fits have been found over a mass range $27 \leqslant A \leqslant 238$. The global prescrip-

tions L and F encompass more cross sections for light targets as the energy approaches 90 MeV, and do well for the polarizations in the middle of the energy range. While the values of most optical model parameters depend strongly on the details of the parametrization, a few quantities appear to be deduced reliably for potentials of Woods-Saxon shape. The real and imaginary rms radii are sharply defined in the fitting and tend to agree closely with values obtained elsewhere for individual best fits. In the energy range analyzed the real rms radii grow slightly but distinctly with E, whereas the imaginary ones fall with E while still remaining larger that the real ones (Fig. 9). A slightly weaker statement can be made for the deduced real and imaginary volume integrals. Consistency of values deduced from the global analysis with those derived from best-fit potentials is good at higher energies, but variable at lower energies, and clearly dependent on the same solution to the discrete potential ambiguities. Much less consistent agreement with other work is found at energies below 15 MeV (see Figs. 11 and 12). In the range $12 \leqslant E \leqslant 90$ MeV our real volume integrals show a 16%, nearly linear falloff with E, while the imaginary volume integrals are almost constant with E for the heavier targets. Our analysis suggests a shift from nearly pure surface absorption at 12 MeV to almost equal parts of surface and volume absorption at 90 MeV; however, the details of this transition are less certain than other parameters.

In Sec. II G we discussed our partial failure to closely reproduce the 22 and 25 MeV reaction cross section data. New data at these and higher energies are greatly needed.

Owing to the scarcity of published data above 15 MeV and the limitations of time, we did not analyze or consider tensor polarization data. While the addition of a small tensor potential term to potential L or F is not expected to materially change the fits presented here, it would be essential to fit or predict such data.[5,64] It is noted that this topic and improvements in the understanding of vector polarization demand and deserve much additional work. Experimental and theoretical studies of tensor and vector polarizations at 80 MeV are planned for the near future in collaboration with the Indiana group.

Note added in proof. A recent study (unpublished) with 52 MeV vector-polarized deuterons by G. Mairle, K. T. Knöpfle, H. Riedesel, G. J. Wagner, V. Bechthold, and L. Friedrich finds good fits to their analyzing powers with $r_{LS} \approx 1.2$ fm and $a_{LS} \approx 0.4$ fm in their parameter set characterized by $r_0 = 1.15$. No imaginary $\vec{L} \cdot \vec{S}$ term was needed.

Potential F of our study yields predictions that fit their data with $\chi^2 = 7.2$. Potential F' has a very small imaginary $\vec{L} \cdot \vec{S}$ term at this energy and does only marginally better with $\chi^2 = 6.2$. χ^2 is defined as in Table II.

ACKNOWLEDGMENTS

*Present address: Goddard Space Flight Center, Code 681, Bldg. 21, Greenbelt, Md. 20770.

[1] S. Watanabe, Nucl. Phys. **8**, 484 (1958).

[2] F. G. Perey and G. R. Satchler, Nucl. Phys. **A97**, 515 (1967).

[3] R. C. Johnson and P. J. R. Soper, Phys. Rev. C **1**, 976 (1970).

[4] R. C. Johnson and P. J. R. Soper, Nucl. Phys. **A182**, 619 (1972).

[5] P. W. Keaton and D. D. Armstrong, Phys. Rev. C **8**, 1692 (1973).

[6] J. M. Lohr and W. Haeberli, Nucl. Phys. **A232**, 381 (1974).

[7] G. H. Rawitscher, Phys. Rev. C **9**, 2210 (1974).

[8] G. H. Rawitscher and S. N. Mukherjee, Phys. Rev. Lett. **40**, 1486 (1978); Ann. Phys. (N.Y.) **122**, 1 (1979).

[9] W. S. Pong and N. Austern, Ann. Phys. (N.Y.) **93**, 369 (1975).

[10] A. A. Ioannides and R. C. Johnson, Phys. Lett. **61B**, 4 (1976).

[11] N. Austern, Phys. Lett. **61B**, 7 (1976).

[12] N. Austern, C. M. Vincent, and J. P. Farrell, Ann. Phys. (N.Y.) **114**, 93 (1978); **96**, 333 (1976).

[13] N. Austern, J. P. Farrell, K. Kabir, and C. M. Vincent, Phys. Rev. C **18**, 1577 (1978).

[14] H. Amakawa et al., Phys. Lett. **82B**, 13 (1979).

[15] G. Baur, R. Shyam, F. Rösl, and D. Trautman (unpublished).

[16] R. M. Drisko, G. R. Satchler, and R. H. Bassel, Phys. Lett. **5**, 347 (1963).

[17] C. M. Perey and F. G. Perey, Phys. Rev. **132**, 755 (1963); C. M. Perey d F. G. Perey, Phys. Rev. **134**, B353 (1964).

[18] F. A. Brieva and J. R. Rook, Nucl. Phys. **A307**, 493 (1978).

[19] J. P. Jeukenne, A. Lejeuen, and C. Mahaux, Phys. Rev. C **16**, 88 (1977); C. B. Dover and N. V. Giai, Nucl. Phys. **A190**, 373 (1972); M. Jaminon, C. Mahaux, and P. Rochus, Phys. Rev. Lett. **43**, 1097 (1979).

[20] A. Nadasen, P. Schwandt, P. P. Singh, A. D. Bacher, W. W. Jacobs, M. D. Kaitchuk, and J. T. Meek (unpublished).

[21] F. G. Perey, Phys. Rev. **131**, 745 (1963).

[22] F. D. Becchetti and G. W. Greenlees, Phys. Rev. **182**, 1190 (1969).

[23] W. W. Daehnick and R. M. DelVecchio, Phys. Rev. C **11**, 623 (1975); R. M. DelVecchio and W. W. Daehnick, ibid. **6**, 2095 (1972); J. R. Shepard, P. D. Kunz, and J. J. Kraushaar, Phys. Lett. **56B**, 135 (1975).

[24] F. Hinterberger, G. Mairle, U. Schmidt-Rohr, and G. J. Wagner, Nucl. Phys. **A111**, 265 (1968).

[25] E. Newman, L. C. Becker, and B. M. Preedom, Nucl. Phys. **A100**, 225 (1967).

[26] G. Perrin et al., Nucl. Phys. **A282**, 221 (1977).

[27] G. Igo, W. Lorenz, and U. Schmidt-Rohr, Phys. Rev. **124**, 832 (1961).

[28] W. Fitz, J. Heger, R. Santo, and S. Wenneis, Nucl. Phys. **A143**, 113 (1970).

[29] M. Takeda, J. Phys. Soc. Jpn. **15**, 557 (1960).

[30] P. R. Christensen, A. Berinde, I. Neamy, and N. Scintei, Nucl. Phys. **A129**, 337 (1969).

[31] N. Cindro and N. S. Wall, Phys. Rev. **119**, 1340 (1960).

[32] A. N. Vereshehagin, O. F. Nemets, L. S. Sokolov, I. P. Chernov, and A. A. Yatis, Izv. Akad. Nauk SSSR, Ser. Fiz. **32**, 1956 (1968). [Bull. Acad. Sci. USSR, Phys. Ser. **32**, 1800 (1968)].

[33] S. A. Hjorth, E. K. Lin, and A. Johnson, Nucl. Phys. **A116**, 1 (1968).

[34] R. K. Jolly, E. K. Lin, and B. L. Cohen, Phys. Rev. **130**, 2391 (1963).

[35] J. L. Yntema, Phys. Rev. **113**, 261 (1959).

[36] H. R. E. Tjin a Djie, F. Udo, and L. A. Ch. Koerts, Nucl. Phys. **53**, 625 (1964); Nucl. Phys. **74**, 417 (1965).

[37] J. Testoni, J. Rosenblatt, and S. Mayo, Nucl. Phys. **74**, 481 (1965).

[38] J. D. Childs, W. W. Daehnick, and M. J. Spisak, Phys. Rev. C **10**, 217 (1974).

[39] G. Duhamel et al., Nucl. Phys. **A174**, 485 (1971).

[40] O. Aspelund et al., Nucl. Phys. **A253**, 263 (1975).

[41] A. Kiss et al., Nucl. Phys. **A262**, 1 (1976).

[42] C. C. Foster, J. C. Collins, D. L. Friesel, W. W. Jacobs, W. P. Jones, S. Kailas, M. Kaitchuck, P. Schwandt, and W. W. Daehnick, Bull. Am. Phys. Soc. **24**, 594 (1979); **24**, 838 (1979).

[43] H. R. Bürgi et al., Nucl. Phys. **A247**, 322 (1975); **A307**, 91 (1978), and **A321**, 445 (1979).

[44] J. Bojowald, C. Mayer-Böricke, M. Rogge, V. Schwinn, and P. Turek, Annual reports KFA Jülich, 1974, 1976, 1978 (unpublished).

[45] P. E. Hodgson, The Optical Model of Elastic Scattering

(Clarendon, Oxford, 1963); Adv. Phys. 15, 329 (1966); N. Austern, *Direct Nuclear Reactions Theories* (Wiley-Interscience, New York, 1970), Chap. 5.

[46]C. M. Perey and F. G. Perey, Phys. Rev. 152, 923 (1966).

[47]G. R. Satchler, Nucl. Phys. 85, 273 (1966).

[48]P. Schwandt and W. Haeberli, Nucl. Phys. A132, 401 (1969).

[49]C. M. Perey and F. G. Perey, At. Data Nucl. Data Tables 17, 1 (1976).

[50]G. R. Satchler, Nucl. Phys. 21, 116 (1960).

[51]Optical model search code GENOA, 1969, written by F. G. Perey (unpublished). The code was modified slightly to adapt it to the characteristics of the DEC 10 system at the University of Pittsburgh.

[52]J. D. Childs, Ph.D. thesis, University of Pittsburgh, 1976 (unpublished).

[53]J. Childs and W. W. Daehnick, Bull. Am. Phys. Soc. 20, 626 (1975).

[54]R. A. Hardekopf, D. D. Armstrong, L. L. Catlin, P. W. Keaton, Jr., and G. P. Lawrence, Los Alamos Report No. LA-5051 (1972).

[55]R. Roche, N. VanSen, G. Perrin, J. C. Gondvand,

A. Fiore, and H. Muller, Nucl. Phys. A220, 381 (1974).

[56]Search code CUPID, written by J. R. Comfort, Univ. of Pittsburgh (unpublished). The code employs a formalism similar to DWUCK (written by P. D. Kunz, Univ. of Colorado), but has a search routine which permits simultaneous fits to polarizations and cross sections for a single target and energy.

[57]B. Wilkens and G. Igo, Phys. Lett. 3, 48 (1962).

[58]S. Mayo, W. Schimmerling, and M. J. Sametband, Nucl. Phys. 62, 393 (1965).

[59]L. R. B. Elton, *Introductory Nuclear Theory* (Pitman, New York, 1965).

[60]See, for instance, A. Bohr and B. R. Mottelson, *Nuclear Structure* (Benjamin, New York, 1969), Vol. 1, p. 187.

[61]L. D. Knutson and W. Haeberli, Phys. Rev. Lett. 30, 986 (1973). L. D. Knutson and W. Haeberli, Phys. Rev. C 12, 1469 (1975).

[62]R. P. Goddard and W. Haeberli, Phys. Rev. Lett. 40, 701 (1978); Nucl. Phys. A316, 116 (1979).

[63]W. H. Wong and P. A. Quin, Bull. Am. Phys. Soc. 24, 846 (1979).

[64]J. R. Frick *et al.*, Phys. Rev. Lett. 44, 14 (1980).